Available online at www.sciencedirect.com

SCIENCE DIRECT®

Vision Research 46 (2006) 902–913

Vision Research

www.elsevier.com/locate/visres

The visual evoked potential in the mouse—Origins and response characteristics

W.H. Ridder III [a], S. Nusinowitz [b,*]

[a] Southern California College of Optometry, Fullerton, CA, USA
[b] Jules Stein Eye Institute, UCLA School of Medicine, Los Angeles, CA, USA

Received 29 July 2005; received in revised form 5 September 2005

Abstract

The visual evoked potential (VEP) in the mouse is characterized and compared to responses obtained with the electroretinogram (ERG). The results indicate that: 1, the VEP originates in the visual cortex; 2, the rod and cone pathways contribute separately to the VEP; 3, temporal tuning functions for rod and cone ERGs are low pass and band pass, respectively; VEP tuning functions are both band pass; and 4, VEP acuity is 0.62 ± 0.156 cycles/degree. The differences in the spatial and temporal tuning functions obtained from the retina and visual cortex provides a tool to investigate signal processing through the visual system.

Keywords: Electroretinogram; Visual evoked potential; Mouse; Temporal; Spatial; Sweep; Acuity; Electrophysiology

1. Introduction

The mouse has become one of the primary models to study visual system disease. While small in comparison to humans, the mouse eye is remarkably similar in structure to humans, sharing similar cell types and structural features. Correspondingly, the visual pathway from the retina to the visual cortex also shares many similarities with that of humans. As a result, both species have many comparable visual disorders and studies in the mouse have led to a better understanding of the sites and mechanisms of disease action in humans. Moreover, because the mouse and human genome share many conserved regions, the mouse has proven to be a highly effective animal model for finding genes relevant to human disease (for example, Chang et al., 2002).

The preferred method for evaluating retinal function is with the electroretinogram (ERG) which is an electrical signal that represents the massed response of the retina to light stimulation. The ERG is easily recorded from the corneal surface of the mouse eye (Nusinowitz, Ridder, & Heckenlively, 2002; Peachey & Ball, 2003) and is commonly used to assess the integrity of the inner, middle, and outer retinal layers.

Post-retinal function can be assessed objectively with the visual evoked potential (VEP). The VEP is a gross electrical potential recorded from the visual cortex in response to a visual stimulus. To obtain a normal VEP requires an intact visual pathway from the retina to the primary visual cortex (Brigell, 2001). Thus, any visual pathway disease (e.g., optic neuritis) that alters the function of the central visual pathway will affect the VEP response.

VEPs have been recorded from the mouse. However, in most instances, VEP stimuli have been limited to brief flashes of light at one or more intensities and one or two temporal frequencies (Chow et al., 2005; Green, Tejada, & Glover, 1994; Henry & Rhoades, 1978; Lehman & Harrison, 2002; Peachey, Roveri, Messing, & McCall, 1997; Ren, LaVail, & Peachey, 2000; Tebano, Luzi, Palazzesi, Pomponi, & Loizzo, 1999). VEP recordings to pattern stimulation in the mouse have been reported (Porciatti, Pizzorusso, & Maffei, 1999a; Porciatti, Pizzorusso, &

* Corresponding author. Tel.: +1 310 206 0496; fax: +1 310 206 3965.
E-mail address: nusinowitz@jsei.ucla.edu (S. Nusinowitz).

0042-6989/$ - see front matter © 2005 Elsevier Ltd. All rights reserved.
doi:10.1016/j.visres.2005.09.006

Maffei, 1999b). However, in the latter studies, recording electrodes were chronically implanted in the visual cortex following craniotomies. The majority of the flash VEP studies used recording electrodes that were inserted subcutaneously over the visual cortex of the skull (but see Tebano et al., 1999) and this particular methodology is desirable because it is non-invasive and provides the potential to rapidly characterize the visual pathway of the mouse.

VEP recordings are currently under-utilized in the mouse. This is, in part, due to a number of technical questions that remain unresolved. For example, in VEP recordings using surface or subcutaneous electrodes, are the recorded signals generated within the visual cortex or are they referred ERGs passively transmitted through the soft tissue of the skull? How do the rod and cone systems contribute to the VEP response? Is the VEP in the mouse sufficiently sensitive to detect differences in the stimulus intensity, and the spatial and temporal properties of the visual pathway, and how do these measurements compare with those made with more invasive procedures, such as craniotomies and/or penetrating electrodes?

The purpose of this study is to determine the cellular origins of the VEP response in the mouse and to characterize these responses. To this end, mice with different mutations affecting specific cells or sites in the retina are used to evaluate the source and contributors to the VEP. Comparisons between the ERG and VEP intensity–response and temporal tuning functions are made to characterize retinal and visual pathway function for both rod- and cone-mediated systems. Finally, mouse spatial tuning functions and visual acuity are assessed with the sweep VEP.

2. Methods

2.1. Mouse strains

All mice were inbred strains obtained from the Jackson Laboratories (Bar Harbor, Maine). Twenty-eight mice (19 C57BL/6J, 5 Cpfl1, 4 *Nob3*) were used in this study. The C57BL/6J mice (hereafter referred to as *B6*) are normal pigmented inbred mice. The *Nob3* mouse is a natural mutant discovered in the screening of mice stock at the Jackson laboratories. The *Nob3* mouse exhibits a selective loss of the *b*-wave of the ERG (Chang et al., 2004). The *Nob3* phenotype is caused by an autosomal recessive mutation that maps to chromosome 11 where the γ-aminobutyric acid (GABA-A) receptor, subunit α6 (Gabra6) gene is located. Sequence analysis identified a missense mutation in exon 3 of the *Gabra6* gene as the cause of the *Nob3* phenotype. A two base substitution was found at position 163–164 (GT to CC) of exon 3. The Cpfl1 mouse (cone photoreceptor function loss 1) has a normal fundus but ERGs do not show a cone mediated response (Chang et al., 2002). The rod mediated ERG is normal. These mice exhibit a progressive cone degeneration with non-detectable cone signals at 2 months of age. This is an autosomal recessive condition that maps to chromosome 19 in the mouse. The phenotypic characteristics of Cpfl1 mice are similar to those observed in patients with complete achromatopsia (ACHM2, OMIM 216900). All animals were 3–6 months of age during testing. All experimental procedures were carried out in compliance with the guidelines on animal experimentation set forth by the National Institute of Health and by the Association for Research in Vision and Ophthalmology (ARVO).

2.2. ERG and VEP recording methodology

Unless otherwise stated, recording procedures for the ERG and VEP, were identical. Mice were anesthetized with an intraperitoneal injection of xylazine (0.5 mg/cc) and ketamine (1 mg/cc) in normal saline. In adult mice, a dose of 0.1 cc/g body weight was administered. Body temperature was maintained at 38° C with a heating pad. Pupils were dilated with Atropine (1%). For ERG recordings, a gold-wire electrode was placed on the corneal surface of the right eye and referenced to a gold wire in the mouth. A needle electrode in the tail served as the ground. The active electrode for the flash VEP (a steel needle) and the sweep VEP (a 2 mm diameter silver/silver chloride cylinder) was placed 3 mm lateral to lambda over the left cortex (contralateral to the stimulated right eye). This location overlies the area of the striate cortex represented by the binocular visual field (Drager, 1975). The reference electrode was a needle electrode placed in the snout or the mouth. The left eye (not stimulated) was occluded with a dark patch for both the ERG and VEP recordings. Responses were amplified (CP511 AC Amplifier, Grass Instruments, Warwick, RI; X 10,000) band pass filtered (1–300 Hz), digitized using an I/O board (Lab-PC-1200, National Instruments, Austin, TX) in a personal computer, and averaged. For the sweep VEP, stimulus production and data collection were carried out with the Enfant (Neuroscientific, Farmingdale, NY) system. The signal was amplified 10,000×, band pass filtered (0.5–100 Hz) and digitized at 300 Hz with 12 bits resolution.

2.2.1. VEP and ERG intensity–response functions

All stimuli were presented in a dome painted with a highly reflective white matte paint (#6080, Eastman Kodak, Rochester, NY). Stimuli were generated with a Grass Photostimulator (PS33 Plus, Grass Instruments, Warwick, RI) affixed to the outside of the dome at 90° to the viewing porthole. Following overnight dark adaptation, rod-mediated responses were recorded to short-wavelength (Wratten 47A; $\lambda_{max} = 470$ nm) flashed stimuli over a 4.0 log unit range of intensities up to the maximum allowable by the photostimulator. Flash intensity was varied in 0.3 log unit intervals using combinations of neutral density filters and intensity settings on the photostimulator control unit. Cone-mediated responses

were obtained with white flashes on a rod-saturating background (32 cd/m^2) and after ten minutes of light adaptation. Responses were computer-averaged at all intensities with up to 50 records averaged for the weakest signals. A signal rejection window was used to eliminate electrical artifacts produced by blinking and eye movements. Flash presentation frequency was set to 1 Hz except at the highest stimulus intensities where flash frequency was 0.2 Hz to avoid adaptation effects.

2.2.2. ERG and VEP temporal response functions

Brief flashes of light were presented at temporal frequencies from 1 to 25 Hz. The light flashes were white with a constant intensity of 1.66 cd-s/m^2. The flash stimuli were presented in the Ganzfeld dome as described above. The mice were dark adapted to obtain rod-mediated temporal response functions and light adapted to obtained cone-mediated temporal response functions (see above).

To eliminate the possibility of contamination that may arise from different flash and background contrast ratios, a flash intensity and background combination was selected for which the contrast ratio was the same under the dark- and light-adapted conditions. To accomplish this, a very weak background was introduced in the dark-adapted state so that a contrast ratio between the flash and the background could be formed. The weak background did not alter the response function from that obtained in complete darkness (data not shown). For both dark- and light-adapted conditions, the contrast ratio was fixed at 0.94 (Michelson contrast ratio).

2.2.3. Sweep VEP

Mice were placed in a stereotaxic (Stoelting, USA) apparatus that held the snout in a fixed position. The mouse was aligned with the stimulus such that the binocular visual field of the right eye was stimulated (i.e., the snout was directed toward the left of the stimulus screen). The average active electrode impedance was $5.2 \pm 2.42\ \mathrm{k\Omega}$ (mean $\pm$ SD, Grass Electrode Impedance Meter, Model EZM3A, Quincy, MA).

The sweep VEP stimulus was a horizontally oriented sine wave grating viewed at 20 cm. The sweep consisted of 11 spatial frequencies (0.10, 0.12, 0.16, 0.20, 0.25, 0.32, 0.40, 0.50, 0.63, 0.80, and 0.98 cpd). The stimulus contrast was 80% and the temporal reversal rate (square wave) was 4 Hz. The screen luminance was 100 cd/m^2 and subtended 100° (H) by 82° (V) at the mouse eye. Each spatial frequency was presented for 1 second so that the entire sweep took 12 seconds (11 spatial frequencies + 1 s pre-adaptation). Sweeps were averaged until the error bars for the data were stable. A similar sweep technique was used to determine contrast thresholds in mice (Lickey, Pham, & Gordon, 2004). Custom made rigid gas-permeable (RGP) contact lenses were placed on the eyes to prevent cataract formation (Ridder, Nusinowitz, & Heckenlively, 2002).

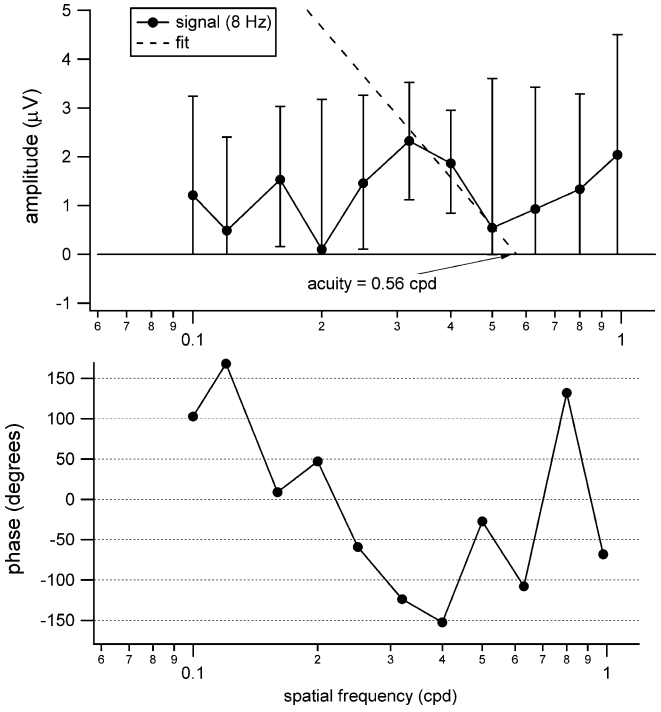

Fig. 1. An example of the visual acuity estimation technique with the sweep VEP. See text for details.

2.2.4. Acuity determination

Fig. 1 displays an example of the acuity extrapolation technique from the sweep VEP. The stimulus spatial frequency is plotted on the horizontal axis and the Fourier derived response amplitude at twice the stimulus fundamental frequency (i.e., 8 Hz) is plotted on the vertical axis for the top graph. The error bars are the 95% confidence intervals. The bottom graph plots the phase response for each spatial frequency. In humans, two methods of acuity extrapolation have been employed (Katsumi, Denno, Arai, De Lopes Faria, & Hirose, 1997; Norcia & Tyler, 1985; Ridder, McCulloch, & Herbert, 1998). Both methods have been shown to give comparable acuity estimates (Ridder, 2004). The method of acuity estimation employed in this study utilized the 95% confidence interval of the signal amplitude as a measure of the noise (Ridder, 2004).

Two methods, that depended on the number of data points above noise, were employed to extrapolate the acuity of a mouse (Ridder et al., 1998; Ridder & Nusinowitz, 2002). The first method utilized a linear fit to the sweep VEP data. Acuities were determined by fitting a line between the high spatial frequency data that were above noise and the first spatial frequency that entered the noise. The data were determined to be noise if the 95% confidence intervals for the sweep VEP amplitude data overlapped with zero. For the set of data shown in Fig. 1, the linear fit to determine the acuity (i.e., the dashed line in the top graph) included data between the peak spatial frequency (0.32 cpd) and the next spatial frequency that was indistinguishable from noise (0.50 cpd). The linear fit was extrapolated to the X-axis (zero amplitude) for the resolution or

visual acuity estimate, which for this mouse was 0.56 cpd (or 20/1071). Human studies indicate that this method of acuity estimation is within one octave of the Snellen acuity (Ridder, 2004). The phase response (bottom graph) gradually becomes more negative until the acuity limit is reached, then it changes randomly. The second method of acuity determination was employed if there were no data points between the peak spatial frequency and the noise level. Under these circumstances, the acuity was taken as the highest spatial frequency response that was above noise. Sweep VEPs were performed on 11 mice in this study. Data from five of the 11 animals tested were adequately fit with a line for the acuity estimate. The acuity estimate for the remaining 6 was taken as the highest spatial frequency above noise. This agrees with the percentage of subjects that produce sweep VEP data that can be fit with a line in human studies (Ridder et al., 1998).

3. Results

3.1. Dark- and light-adapted cortical VEPs

Representative VEPs recorded under dark- (heavy lines) and light- (thin lines) adapted conditions are shown in Fig. 2A. As flash intensity is increased (from bottom to top of figure) the amplitude of the first negative peak (P1-N1) increases and the latency of N1 decreases under both dark- and light-adapted conditions. However, in contrast to the dark-adapted responses, light-adapted responses for the same flash conditions, are smaller in amplitude and, surprisingly, latency is prolonged. The relation between latency and amplitude is shown in Fig. 2B where the filled and open symbols are the responses recorded under dark- and light-adapted conditions, respectively. Data points identified with the same letter are from the same mouse. Comparing the filled and open symbols with the same identifying letters clearly demonstrates that under light-adapted conditions, VEP responses are smaller in amplitude and delayed with respect to the corresponding response under dark-adapted conditions. The relation between amplitude and stimulus intensity is shown in Fig. 2C. Response amplitude increases with flash intensity under dark- and light-adapted conditions, but there is an approximate 2-fold increase in amplitude for the dark- compared to the light-adapted responses for the same stimulus (vertical dashed line).

While the reduced amplitude under light-adapted conditions was not unexpected, the prolonged latencies were surprising. In fact, the light-adapted response to the brightest stimulus appears similar in amplitude and timing to dark-adapted responses obtained to weaker stimuli, possibly suggesting that the rod system is mediating the response to a less effective stimulus even under light-adapted conditions. Experiments to be described below with mutant mice lacking cone photoreceptors (*Cpfl1*) will determine whether cones are mediating the VEP response under light-adapted conditions.

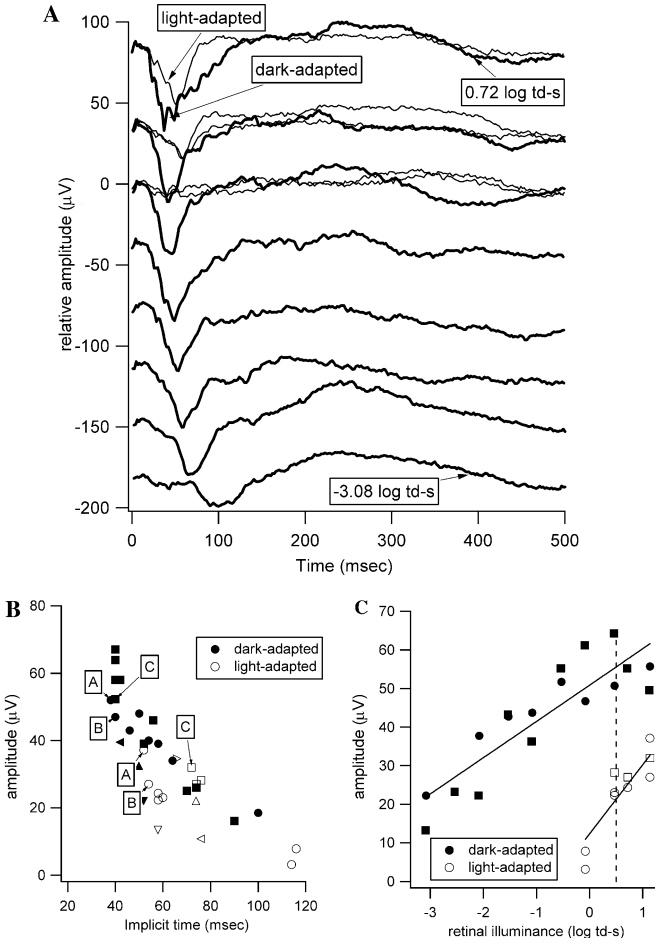

Fig. 2. (A) Full-field flash VEP responses from a B6 mouse under light- and dark-adapted conditions. As the stimulus intensity increases (from the bottom to the top of the figure), the response amplitude (P1-N1) increases and the latency decreases. (B) A plot of the implicit time of N1 versus the amplitude of P1-N1. The light-adapted conditions exhibit a longer implicit time and lower amplitude than the comparable dark-adapted condition. (C) A plot of stimulus intensity versus response amplitude (P1-N1). See text for further details.

3.2. Does the VEP result from passive propagation of the ERG electrical activity?

The mouse ERG is a robust signal. Since the mouse skull is small, it is possible that the VEP is actually a recording of the electrical activity of the ERG on the skull and the changes in signal morphology are related to the delay in signal transmission across the soft tissue of the skull. To test this possibility, the VEP in response to a dim flash (0.1233 cd/m^2) was recorded at several locations between the mouse eye and the contralateral visual cortex (inset Figs. 3A–F). In Fig. 3A, the skin is intact and the recordings were made with a needle electrode penetrating the scalp. In Fig. 3B, the scalp has been resected to expose the skull and the electrode contacted the skull directly. The top trace was obtained with the electrode on the cornea (i.e., an ERG, Position A). The second trace was obtained with the electrode 1 mm

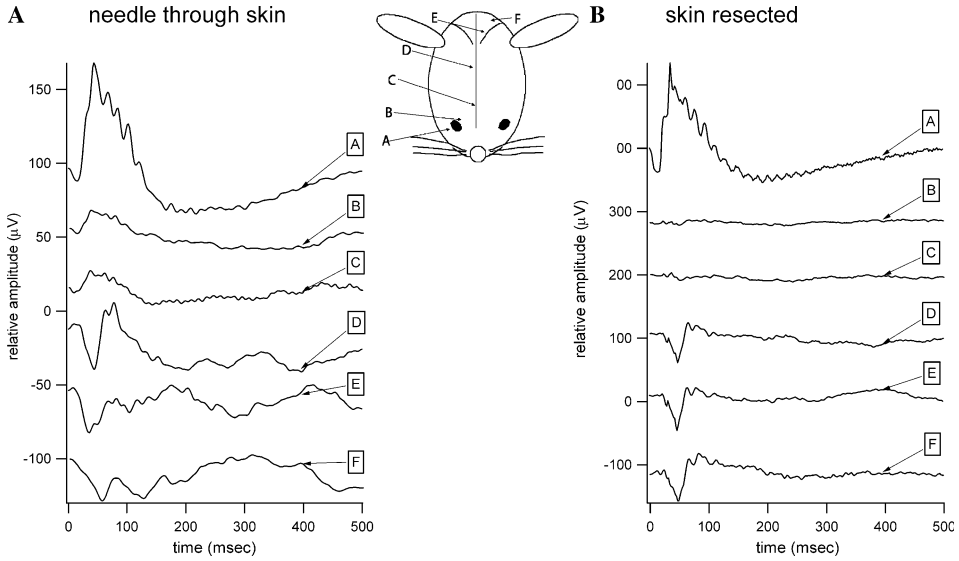

Fig. 3. The effect of active electrode location on the ERG and VEP recording. The active electrode locations are depicted in the mouse diagram and the corresponding recordings obtained with a needle electrode through the skin (A, left data set) or with the skin resected (B, right data set) are displayed. The recordings labeled "A" are ERGs. As the distance from the active electrode and the eye increases, the ERG amplitude decreases. An ERG can not be recorded 1 mm behind the eye with the skin resected. The VEP amplitude increases as the area over the striate cortex is approached. See text for further details.

behind the eye (Position B). Subsequent traces (Positions C–F) approach the contralateral visual cortex. When the skin is intact, the ERG can be recorded several millimeters behind the eye (Fig. 3A). When the skin is resected (Fig. 3B) and the electrode only contacts the skull, the ERG cannot be recorded behind the eye (Positions B and C). This suggests that the electrical activity of the ERG can travel a few millimeters through soft tissue. As the striate cortex is approached, the VEP amplitude increases.

ERG and VEP recordings were made from *Nob3* mice to further investigate the possibility that the VEP is the result of passive propagation of electrical activity from the ERG. Fig. 4 displays the dark-adapted results for 2 *Nob3* mice (m1 and m2). The ERGs (Fig. 4A) indicate that these mice do not have a *b*-wave under dark-adapted conditions. If the VEP is the result of electrical propagation of the ERG through the soft tissue, then the recorded VEP should be similar in appearance to the ERG. The VEP (Fig. 4B) was not recordable under these stimulus conditions.

The experiments described in Figs. 3 and 4 suggest that the VEP is not the result of passive propagation of electrical activity of the ERG recorded at the striate cortex. Thus, the origin of the mouse VEP, like the VEP recorded in the monkey, is in the striate and extra-striate cortex (Dagnelie,

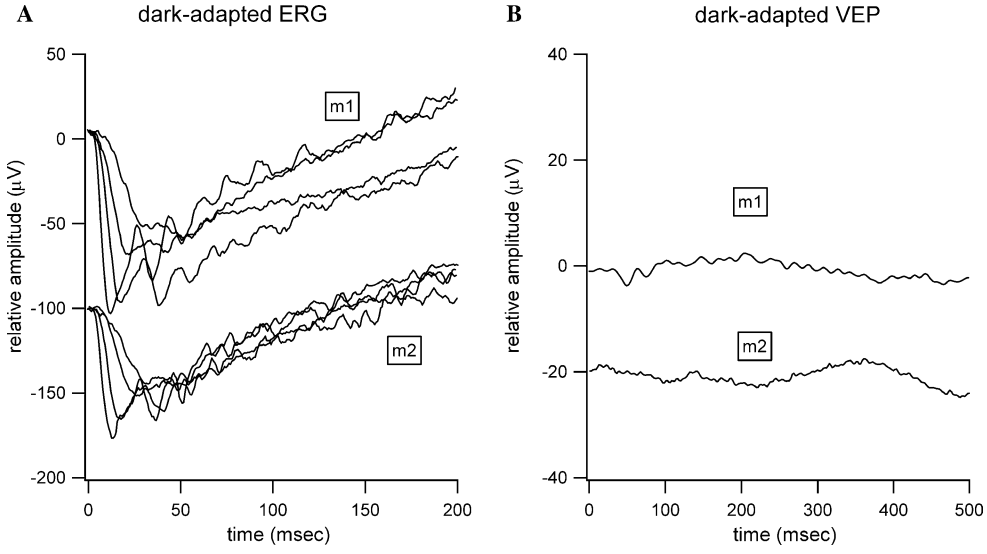

Fig. 4. Dark-adapted ERG (A) and VEP (B) recordings from 2 *Nob3* mice (m1 and m2). The mice do not exhibit a *b*-wave in the ERG and the VEP is not recordable. See text for details.

Spekreijse, & van Dijk, 1989; Kraut, Arezzo, & Vaughan, 1985; Schroeder, Tenke, & Givre, 1992; Schroeder, Tenke, Givre, Arezzo, & Vaughan, 1991; Van der Marel, Dagnelie, & Spekreijse, 1984).

3.3. Light-adapted VEPs and the Cpfl1 mouse

The mouse is primarily a nocturnal animal with a predominantly rod (97%) retina (Carter-Dawson & LaVail, 1979; Szel, Lukats, Fekete, Szepessy, & Rohlich, 2000). However, the data in Fig. 2 demonstrate that the mouse has a dark- and light-adapted VEP that can be of similar amplitude. To determine if the light-adapted VEP is cone driven, the VEP response was recorded from *Cpfl1* mice that do not have cone photoreceptors. Fig. 5 displays the results for one mouse. Fig. 5A contains the dark- and light-adapted ERGs. The dark-adapted ERGs are robust and of normal amplitude but the light-adapted ERGs are non-recordable. Fig. 5B shows the dark- and light-adapted VEPs for the same stimulus conditions. Similar to the ERGs, the dark-adapted VEPs are well-formed but the light-adapted VEPs are non-recordable. Thus, the light-adapted VEP in the mouse is the result of cone photoreceptor activity; no rod input is suggested.

3.4. Rod system ERG and VEP intensity–response functions

Intensity–response functions for rod-mediated ERGs (dashed line) and VEPs (solid line) are shown in Fig. 6. Amplitude of the *b*-wave (ERG) or P1-N1 (VEP) is plotted on the *Y*-axis. Each data set was fitted with the Naka-Rushton function (Penn & Hagins, 1972), shown as a dashed line for the ERG recordings and a solid line for the VEP recordings. The fit of the Naka-Rushton equation provided estimates for V_{max}, the maximum saturated amplitude, and k, the semi-saturation intensity.

V_{max} was significantly higher for ERG recordings than for the VEP recordings under identical stimulus conditions. For the ERG recordings, V_{max} was 302.8 μV, whereas for the VEP recordings, V_{max} was only 56.3 μV ($t = 91.8$,

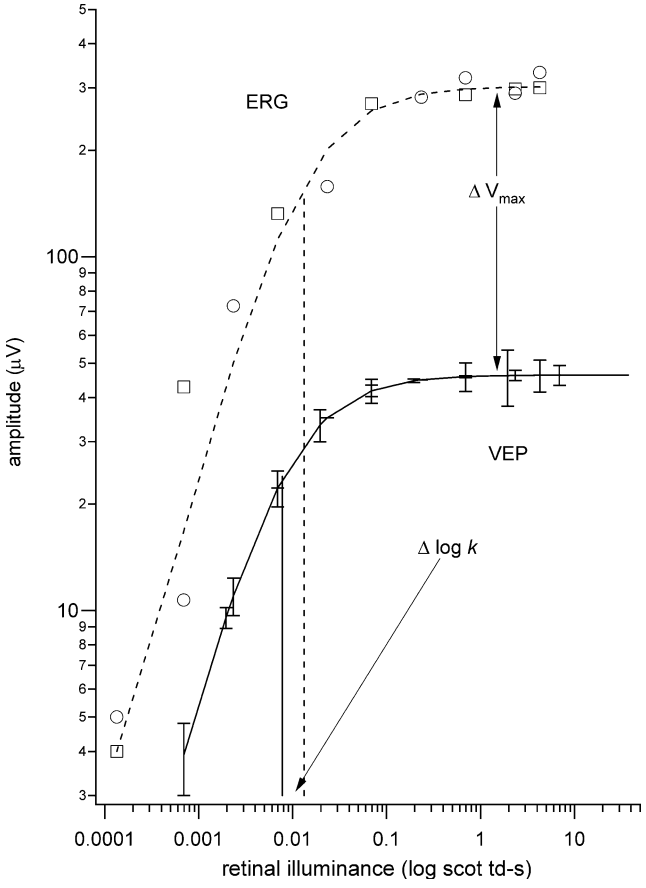

Fig. 6. Intensity–response functions for the ERG (dashed line) and the VEP (solid line) from a B6 mouse. See text for details.

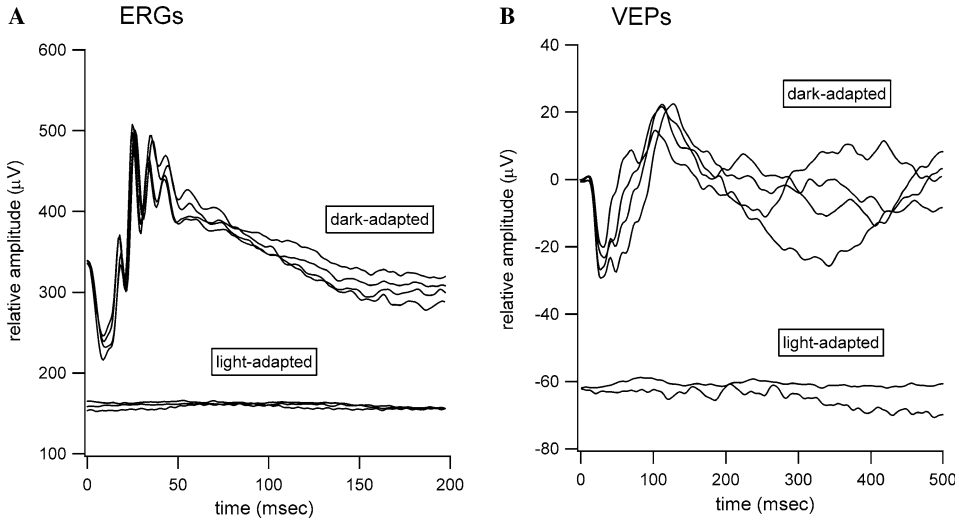

Fig. 5. ERG (A) and VEP (B) recordings from a Cpfl1 mouse. The dark-adapted condition resulted in a normal ERG and VEP. Under light-adapted conditions, neither the ERG nor the VEP were recordable. See text for further details.

$p < 0.0035$). In contrast, k was similar for the ERG and VEP recordings, although there was a slight shift to a lower estimate of k (i.e., a higher sensitivity) for the VEP recordings for the group data. However, a comparison of individual k's obtained for each animal was not statistically different ($t = 5.30$, $p = 0.06$).

3.5. ERG and VEP temporal response functions

ERGs and VEPs were recorded to temporally modulated stimuli as described in Section 2.2.2. The critical flicker fusion frequency (CFF) for rod- and cone-mediated vision was estimated from these response functions (described next). Consider first the ERG data shown in Fig. 7A. Rod ERGs showed a slow roll-off in amplitude as temporal frequency is increased. At the highest temporal frequency, ERG amplitudes were still clearly above noise levels, which we define as 2 μV, the latter determined from recordings in the absence of a visual stimulus. The rod ERG response function is consistent with a low pass temporal response filter. The cone ERG temporal response function (Fig. 7B) is broader than that for rods and is consistent with a band pass filter with a peak sensitivity at approximately 3 Hz. The data were fit with a double-exponential function with four floating variables (peak response amplitude, peak temporal frequency, high temporal frequency slope, and low temporal frequency slope) (Kiorpes, Kiper, & Movshon, 1993). In this model, response amplitude (RA) equals:

$$k_s(ws)^{\alpha}e^{-\beta ws}, \tag{1}$$

where w is the temporal frequency. The four floating variables are: k_s, the peak response amplitude for the function; s, the peak temporal frequency for the function; α which affects the low temporal frequency slope; and β affects the high temporal frequency slope of the function. The dashed curves drawn through the data are the best fits based on this function. The CFF was extrapolated by extending the curve to a response amplitude of 2.0 μV, the average noise level for the ERG. Based on this fit, the CFF was 26.2 Hz for rods and 41.3 Hz for cones. (r^2 describing the fit of the equation to the data was 0.98 and 0.92 for the rod and cone ERGs, respectively.)

The VEP responses for the same mice and stimulus conditions are shown in Fig. 7C. The waveform morphology for the VEP is different from that of the ERG. Rod-mediated VEPs now demonstrate a band pass filtering with a peak response at approximately 2 Hz. Response amplitudes show a slow roll-off on either side of the peak frequency. Cone VEPs show a broad temporal response profile much like the ERG. However, unlike the cone ERGs, the cone VEPs are suggestive of a bi-modal function, with a peak at 2 Hz and another at 4 Hz. Eq. (1) was fitted to the rod- and cone- temporal response functions and extrapolated to 2.4 and 3.7 μV, which is the noise level for rod and cone signals, respectively, to estimate the VEP CFFs. Based on the fit of Eq. (1), the CFF was 7.1 Hz for rods and 9.0 Hz for cones (r^2 describing the fit of the equation to the data was 0.99 and 0.86 for the rod and cone VEPs, respectively).

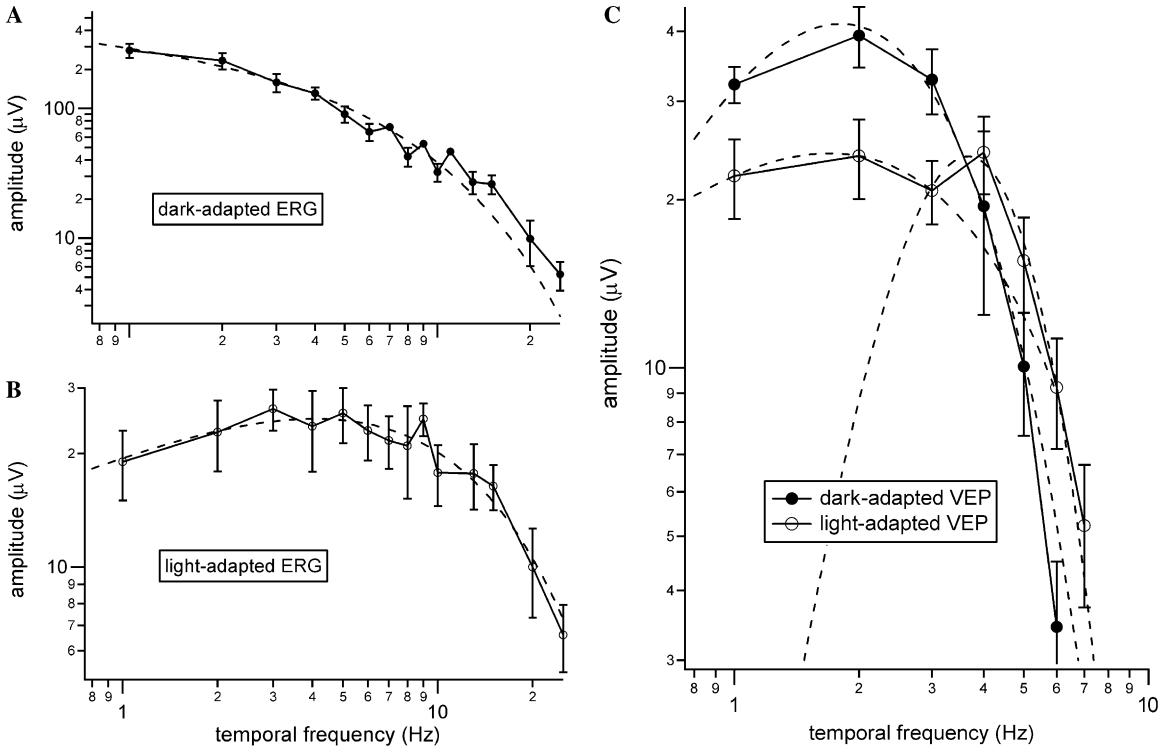

Fig. 7. ERG (A and B) and VEP (C) temporal tuning functions from a B6 mouse under dark- and light-adapted conditions. See text for details.

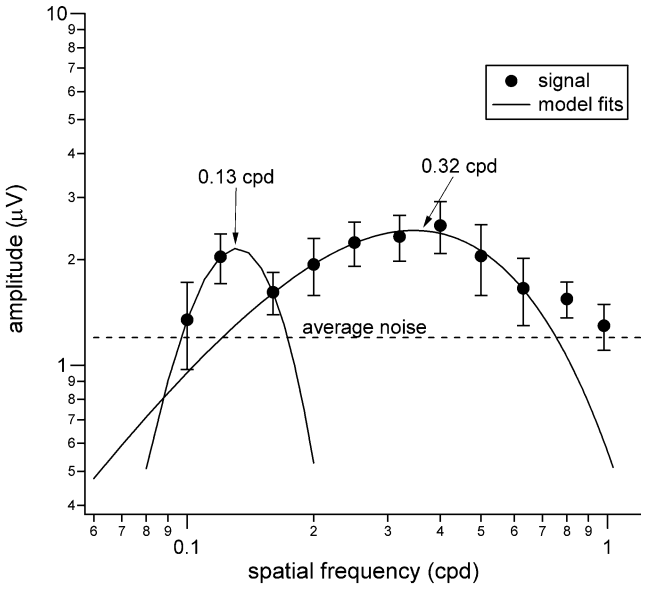

Fig. 8. The average of the sweep VEP data from eleven B6 mice. See text for details.

3.6. Visual acuity

Using the acuity extrapolation technique described in the methods section, the acuity was determined for 11 B6 mice. The average acuity for the B6 mice was 0.62 ± 0.156 cpd (mean $\pm$ SD). This corresponds to a Snellen acuity of 20/968.

3.7. Average sVEP function

Seven of the eleven B6 mice in which sweep VEPs were recorded, displayed a double peaked function. To investigate this double peaked function, the data from all 11 B6 mice were averaged together. Fig. 8 displays the average of the sweep VEP data for the 11 mice. The error bars are the standard error of the mean for the 11 mice. The average noise line is the average of the noise obtained for all of the animals at all of the spatial frequencies. The noise was estimated as the Fourier derived amplitude for a temporal frequency adjacent to two times the stimulus temporal frequency (i.e., adjacent to 2F1). The data were fit with Eq. (1) from above. The data at 0.80 and 0.98 cpd were not included in the fit because they were not significantly different from noise (paired t test for the average signal and noise at these spatial frequencies had $p > 0.05$). The function has peaks at 0.13 and 0.32 cycles per degree.

4. Discussion

4.1. Origin of the VEP in the mouse

The mouse exhibits VEPs under both dark- and light-adapted conditions. By recording VEPs in mice that do not have cones, it was demonstrated that the dark-adapted VEP results from rod activity and the light-adapted VEP results from cone activity (Fig. 5). The VEP amplitude increases as the stimulus intensity increases (Fig. 2). However, the dark-adapted VEP is significantly greater in amplitude than the light-adapted VEP. This suggests that the rod pathway recruits more cortical cells than the cone pathway. In addition, fewer responding cortical cells may explain the temporal response differences (i.e., shorter latencies for the dark adapted VEP) between dark- and light-adapted VEPs.

An electrical charge can travel through conductive media like the soft tissues of the head and the skull. Since the mouse skull is small, the significant electrical activity produced in the retina by visual stimulation may be conducted throughout the skull. This could then be falsely interpreted as a VEP. Several experiments were carried out to test this possibility. Fig. 3 demonstrates that the electrical activity produced in the retina can travel several millimeters. However, this electrical current did not reach the skull over the visual cortex. For example, the mouse examined in Fig. 3B had a normal ERG recording. This animal had an electrically quiet zone approximately one millimeter behind the eye. As the visual cortex was approached, the normal VEP waveform became apparent. Furthermore, if the VEP was the result of the passive flow of electrical charge produced in the retina, then the recorded waveform should remain relatively constant irrespective of the recording location. Fig. 3 demonstrates that the waveform of the ERG and VEP are significantly different. Finally, the experiments described in Fig. 4 demonstrate that even when electrical activity is produced in the retina, if the visual signal is not transmitted centrally through the optic nerve, no VEP will be recorded. This was demonstrated using the *Nob3* mutant mice for which signal transmission from photoreceptors to downstream cells has been disrupted. Thus, the VEP is not the result of the passive flow of electrical charge produced by retinal activity.

4.2. Mouse VEP characteristics

4.2.1. Intensity–response functions

ERGs and VEPs were recorded to identical flashed stimuli of varying intensity. Peak-to-peak (i.e., *b*-wave) amplitudes of the ERG demonstrated the typical pattern of a linear increase over low intensities followed by a non-linear region over which amplitudes did not change. VEP responses demonstrated the same pattern when P1-N1 amplitude was plotted against flash intensity. The intensity range over which responses were saturated was similar for the ERG and VEP, although the range was slightly broader for the VEP recordings (Fig. 6). In addition, VEP amplitudes were always of smaller magnitude compared to the ERG, a finding that is consistent with prior reports in which ERG and VEP recordings were made to the same stimuli (Goto, Taniwaki, Shigematsu, & Tobimatsu, 2003; Hayton, Kriss, Wade, & Muller, 2003; Peachey &

Ball, 2003; Ren et al., 2000). In this study, the threshold intensity sufficient to elicit a just detectable response was almost 1.0 log unit higher for the VEP than for the ERG. The differences between the ERG and VEP amplitudes may be attributable to factors that decrease the signal/noise ratio, such as the number of cells responding at the retina and visual cortex and/or the distance between the recording electrode and the site of the electrical generator for the signal. In our experiments, the recording electrode was inserted subcutaneously over the visual cortex. However, in earlier experiments (not described here), stainless-steel electrodes were implanted in the skull such that the tip of the recording electrode contacted the dura overlying the visual cortex. VEP amplitudes under these conditions were significantly larger than those obtained with our surface electrode, but were still not as large as the ERG recordings, a finding that is also consistent with prior studies in which the active electrode penetrated the skull (Goto et al., 2003; Green et al., 1994).

In contrast to the large differences in VEP and ERG amplitudes, the semi-saturation intensity, k, obtained from the fit of the Naka-Rushton equation, was not significantly different for the two tests (Fig. 6). This would suggest that under these experimental conditions the sensitivity of the visual system to detect differences in stimulus intensity is the same at the level of the retina and the visual cortex.

4.2.2. Temporal tuning functions

Temporal tuning functions were recorded with the ERG and the VEP under dark- and light-adapted conditions. The temporal tuning functions for the ERG were low pass and band pass for the dark- and light-adapted conditions, respectively. Previous reports have suggested low pass (Ekesten, Gouras, & Moschos, 1998; Jaissle et al., 2001) or band pass (Krishna, Alexander, & Peachey, 2002) filtering for light-adapted temporal response functions and low pass for the dark-adapted function (Jaissle et al., 2001).

The ERG CFF in the present study was determined by extrapolating double exponential function fits to the high temporal frequency data noise level. The rod-mediated CFF was 26.2 Hz and the cone-mediated CFF was 41.3 Hz. In previous reports, the mouse cone system has been shown to be capable of responding to temporal frequencies up to 50 Hz, although the specific CFF was not derived in these studies (Ekesten et al., 1998; Krishna et al., 2002). Most species display lower ERG CFFs for dark-adapted than light-adapted conditions (Ordy & Samorajski, 1968). The mouse ERG dark- and light-adapted CFFs reported here are similar to other rodent species (guinea pig dark- and light-adapted CFFs of 21 and 51 Hz, respectively) (Armitage, Bui, Gibson, & Vingrys, 2001).

The shapes of the temporal tuning functions obtained with the VEP were both band pass. The CFFs were 7.1 and 9.0 Hz for the dark- and light-adapted conditions, respectively. The function shape and the CFF for the light-adapted temporal tuning function agrees with previous reports employing flash and pattern VEPs (Porciatti et al., 1999b; Strain & Tedford, 1993). Porciatti et al. (1999b) stated that under light adapted conditions the temporal tuning function had a peak at 2–4 Hz and the CFF was about 12 Hz. (Porciatti et al., 1999b).

Temporal tuning functions have also been recorded from single cells in the dorsal lateral geniculate nucleus (dLGN) of the mouse (Grubb & Thompson, 2003). Most of the cells recorded from in the dLGN exhibited band pass tuning functions. Thus, the change in the shape of the dark-adapted function from low pass (ERG) to band pass (VEP) is due to either ganglion cell or dLGN cell processing. The average peak of the function for single dLGN cells was 3.95 ± 0.24 Hz which agrees with the peak of the temporal tuning functions determined with the VEP (i.e., 2–4 Hz). The average high temporal frequency cut off for the dLGN cells was 7.26 ± 0.40 Hz. However, Fig. 7C of Grubb and Thompson (2003) clearly display a bimodal function with several cells having higher temporal frequency cut offs. Thus, the temporal capabilities of dLGN cells in the mouse mirror the observations with the VEP.

By examining the relative amplitude change for the light- and dark-adapted conditions for the ERG and VEP, assumptions about the processing of cone and rod information can be made. The ERG/VEP amplitude ratio at the peak frequency of the VEP (about 2 Hz) is approximately 7/1 for rods and 1/1 for cones. However, at 6 Hz, the ERG/VEP ratios are approximately 7/1 for rods and 6/1 for cones. On the assumption that signal amplitude is proportional to the number of cells responding at the retina and visual cortex, the difference in the rod and cone ERG/VEP ratios suggests that the rod pathway has a significant amount of information convergence between the retina and the cortex at lower temporal frequencies, whereas, the cone pathway does not. This presumed information convergence disappears at the higher temporal frequencies. Additionally, the rod-mediated VEP amplitude is greater than the cone VEP amplitude at lower temporal frequencies (up to 4 Hz) but not at higher temporal frequencies. This means that the rod pathway recruits more cortical cells than the cone pathway at lower temporal frequencies, whereas relatively more cone driven cortical cells are recruited at higher temporal frequencies.

4.2.3. Visual acuity

By employing the methodology outlined in Fig. 1, the average sweep VEP acuity for all of the mice was 0.62 ± 0.156 cpd (mean $\pm$ SD, $N = 11$). This acuity agrees well with previous estimates of the visual acuity of mice using invasive procedures. Using a pattern VEP technique, the acuity of normal mice was found to be either 0.60 ± 0.15 cpd (mean $\pm$ SD, $N = 10$) (Porciatti et al., 1999b) or 0.59 ± 0.08 cpd (mean $\pm$ SD, $N = 16$) (Rossi et al., 2001). The VEP acuities also agree with previous pattern ERG measures of acuity (Porciatti, Pizzorusso, Cenni, & Maffei, 1996; Rossi et al., 2001).

Several psychophysical methods have also been used to measure the visual acuity of mice (Gianfranceschi, Fiorentini, & Maffei, 1999; Prusky, Alam, Beekman, & Douglas, 2004; Prusky, West, & Douglas, 2000; Schmucker, Seeliger, Humphries, Biel, & Schaeffel, 2005). Gianfranceschi et al. (1999), by employing a double corridor maze, found the visual acuity of normal mice to be 0.51 ± 0.08 cpd (mean $\pm$ SD, $N = 4$). Prusky et al. (2000) employed a water maze, which resulted in an average acuity estimate of 0.49 ± 0.03 cpd (mean $\pm$ SD, $N = 15$). By employing an optometer testing apparatus, the visual acuity of the mouse has been determined to be about 0.4–0.5 cpd (Prusky et al., 2004; Schmucker et al., 2005).

The psychophysical measures of visual acuity agree well with the electrophysiological measures in normal mice. Methodological differences could account for the VEP acuities being slightly higher than the psychophysical acuities. In the psychophysical studies employing mazes, the acuity was taken as the 70% correct level on the psychometric function, whereas, the electrophysiological studies extrapolated the high spatial frequency amplitude data to the *X*-axis for an acuity estimate. This may result in a slightly higher estimate of acuity with the VEP techniques. Thus, the sweep visual evoked potential can be used to obtain accurate acuity estimates in mice. Furthermore, the sweep VEP estimate of acuity can be obtained much quicker (<1 h) than the psychophysical estimates which may take several weeks of training and testing.

The sweep VEP acuity estimates are also similar to the acuities determined from single cell recordings from retinal ganglion cells and lateral geniculate nucleus (dLGN) cells. Single cell recordings from the mouse retinal ganglion cells and the dLGN examined the spatial properties of individual neurons (Grubb & Thompson, 2003; Stone & Pinto, 1993). The retinal ganglion cells displayed an average high spatial frequency cut off of 0.20 ± 0.014 cpd, however, some cells had cut offs as high as 0.425 cpd (Stone & Pinto, 1993). The spatial frequency tuning functions for the retinal ganglion cells were low pass (Stone & Pinto, 1993). Most dLGN cells displayed a band pass spatial frequency tuning function (Grubb & Thompson, 2003). The average peak of the function was 0.027 cpd and the average high spatial frequency cut off was 0.18 cpd. However, cells with cut offs as high as 0.53 cpd were identified. Thus, single cell recordings from retinal ganglion cells and dLGN cells resulted in acuity estimates similar to those obtained with VEPs and psychophysical techniques.

4.2.4. Average sVEP function

The averaged sweep VEP function from the 11 B6 mice displayed a double peaked function (Fig. 8). A double peaked function has also been observed in human sweep VEP recordings (Gottlob, Wizov, Odom, & Reinecke, 1993; Strasburger, Scheidler, & Rentschler, 1988). In human studies, this double peaked function has been postulated to be the result of the interaction of visual information in two parallel channels (e.g., the transient and sustained channels) reaching the cortex out of phase. This is the result of the two channels having different spatial and temporal processing abilities. Transient and sustained or Y-like and X-like visual cells were also identified in the mouse (Balkema & Pinto, 1982; Grubb & Thompson, 2005; Stone & Pinto, 1993). Thus, the double peaked function in the mouse may be the result of two parallel channels of information flow. At intermediate spatial frequencies (around 0.2 cpd), the information from the two channels may interact destructively to produce a decrease in signal amplitude at the striate cortex.

Examining the average sVEP function and comparing it with the known anatomical properties of cells in the mouse visual pathway may reveal which cell types are responsible for the double peaked sVEP function. Anatomically, three classes of monostratified ganglion cells have been identified in the mouse retina (RG_A, RG_B, and RG_C) (Diao, Sun, Deng, & He, 2004; Peichl, Ott, & Boycott, 1987; Sun, Li, & He, 2002). The RG_A cells have large cells bodies and dendritic spreads, the RG_B cells have small to medium sized cells bodies and dendritic spreads, and the RG_C cells have small to medium sized cell bodies with medium to large dendritic spreads. Based on these anatomical observations, the RG_A cells should respond best to low spatial frequency and high temporal frequency stimuli. The RG_B and RG_C cells should respond best to higher spatial and lower temporal frequencies. Sun et al. (2002) suggested that the RG_{A1} cell is the α-cell identified in other species (e.g., the cat) that may be a Y-like cell. They also suggested that the RG_{B2} cell may be similar to the β-cell of the rabbit (i.e., X-like). The average dendritic spreads for the RG_{A1} and RG_{B2} cells are 318 and 135 μ, respectively (Sun et al., 2002). The spatial resolution for these cells can be determined from the schematic eye formulas for the mouse developed by Remtulla and Hallett (1985). Using these formulas, the spatial resolution capability for the RG_{A1} and RG_{B2} cells are 0.049 and 0.11 cpd, respectively. Thus, the RG_{A1} cells may be responsible for the low spatial frequency peak and the RG_{B2} cells for the higher spatial frequency peak of the sweep VEP function.

4.3. Summary

In summary, the results of these studies indicate that the VEP is not the result of the ERG response propagated passively through the soft tissue of the skull. Experiments with the *Cpfl1* mutant mice lacking cones demonstrate that cones contribute to the VEP response under light-adapted conditions. Spatial and temporal VEP tuning functions agree with previous reports as well as with single cell results and the mouse visual acuity can be easily and reliably determined with the sweep VEP. These results suggest that the flash and sweep VEP can be used to assess the visual pathway of the mouse from the retina to the striate cortex.

Acknowledgments

Special thanks to Drs. B. Chang and J. Heckenlively for providing the mutant mice used in some of these studies. Supported by grants from the Kirchgessner Foundation and Research to Prevent Blindness (S.N.).

References

Armitage, J. A., Bui, B. V., Gibson, R., & Vingrys, A. J. (2001). Postnatal development of flicker sensitivity in guinea pigs. *Clinical and Experimental Optometry, 84*(5), 270–325.

Balkema, G. W., Jr., & Pinto, L. H. (1982). Electrophysiology of retinal ganglion cells in the mouse: A study of a normally pigmented mouse and a congenic hypopigmentation mutant pearl. *Journal of Neurophysiology, 48*(4), 968–980.

Brigell, M. (2001). The visual evoked potential. In G. Fishman, D. Birch, G. E. Holder, & M. Brigell (Eds.), *Electrophysiologic testing in disorders of the retina, optic nerve, and visual pathway* (pp. 237–279). San Francisco: The Foundation of the American Academy of Ophthalmology.

Carter-Dawson, L. D., & LaVail, M. M. (1979). Rods and cones in the mouse retina I. Structural analysis using light and electron microscopy. *Journal of Comparative Neurology, 188*(2), 245–262.

Chang, B., Hawes, N. L., Hurd, R. E., Davisson, M. T., Nusinowitz, S., & Heckenlively, J. R. (2002). Retinal degeneration mutants in the mouse. *Vision Research, 42*(4), 517–525.

Chang, B., Hawes, N. L., Hurd, R. E., Wang, J., Davisson, M. T., Nusinowitz, S., et al. (2004). Selective loss of ERG b-wave caused by an autosomal recessive mutation in mice. *Investigative Ophthalmology &Visual Science, 45*, 41.

Chow, E., Mottahedeh, J., Prins, M., Ridder, W., Nusinowitz, S., & Bronstein, J. M. (2005). Disrupted compaction of CNS myelin in an OSP/Claudin-11 and PLP/DM20 double knockout mouse. *Molecular and Cellular Neuroscience, 29*(3), 405–413.

Dagnelie, G., Spekreijse, H., & van Dijk, B. (1989). Topography and homogeneity of monkey V1 studied through subdurally recorded pattern-evoked potentials. *Visual Neuroscience, 3*(6), 509–525.

Diao, L., Sun, W., Deng, Q., & He, S. (2004). Development of the mouse retina: Emerging morphological diversity of the ganglion cells. *Journal of Neurobiology, 61*(2), 236–249.

Drager, U. C. (1975). Receptive fields of single cells and topography in mouse visual cortex. *Journal Comparative Neurology, 160*(3), 269–290.

Ekesten, B., Gouras, P., & Moschos, M. (1998). Cone properties of the light-adapted murine ERG. *Documenta Ophthalmologica, 97*(1), 23–31.

Gianfranceschi, L., Fiorentini, A., & Maffei, L. (1999). Behavioural visual acuity of wild type and bcl2 transgenic mouse. *Vision Research, 39*(3), 569–574.

Goto, Y., Taniwaki, T., Shigematsu, J., & Tobimatsu, S. (2003). The long-term effects of antiepileptic drugs on the visual system in rats: Electrophysiological and histopathological studies. *Clinical Neurophysiology, 114*(8), 1395–1402.

Gottlob, I., Wizov, S. S., Odom, J. V., & Reinecke, R. D. (1993). Predicting optotype visual acuity by swept spatial visual-evoked potentials. *Clinical Vision Science, 8*, 417–423.

Green, D. G., Tejada, P., & Glover, M. J. (1994). Herreros de electrophysiological estimates of visual sensitivity in albino and pigmented mice. *Visual Neuroscience, 11*(5), 919–925.

Grubb, M. S., & Thompson, I. D. (2003). Quantitative characterization of visual response properties in the mouse dorsal lateral geniculate nucleus. *Journal of Neurophysiology, 90*(6), 3594–3607.

Grubb, M. S., & Thompson, I. D. (2005). Visual response properties of burst and tonic firing in the mouse dorsal lateral geniculate nucleus. *Journal of Neurophysiology, 93*(6), 3224–3247.

Hayton, S. M., Kriss, A., Wade, A., & Muller, D. P. (2003). The effects of different levels of all-rac- and RRR-alpha-tocopheryl acetate (vitamin E) on visual function in rats. *Clinical Neurophysiology, 114*(11), 2124–2131.

Henry, K. R., & Rhoades, R. W. (1978). Relation of albinism and drugs to the visual evoked potential of the mouse. *Journal of Comparative and Physiological Psychology, 92*(2), 271–279.

Jaissle, G. B., May, C. A., Reinhard, J., Kohler, K., Fauser, S., Lutjen-Drecoll, E., et al. (2001). Evaluation of the rhodopsin knockout mouse as a model of pure cone function. *Investigative Ophthalmology & Visual Science, 42*(2), 506–513.

Katsumi, O., Denno, S., Arai, M., De Lopes Faria, J., & Hirose, T. (1997). Comparison of preferential looking acuity and pattern reversal visual evoked response acuity in pediatric patients. *Graefes Archives Clinical Experimental Ophthalmology, 235*(11), 684–690.

Kiorpes, L., Kiper, D. C., & Movshon, J. A. (1993). Contrast sensitivity and vernier acuity in amblyopic monkeys. *Vision Research, 33*(16), 2301–2311.

Kraut, M. A., Arezzo, J. C., & Vaughan, H. G. Jr., (1985). Intracortical generators of the flash VEP in monkeys. *Electroencephalography and Clinical Neurophysiology, 62*(4), 300–312.

Krishna, V. R., Alexander, K. R., & Peachey, N. S. (2002). Temporal properties of the mouse cone electroretinogram. *Journal of Neurophysiology, 87*(1), 42–48.

Lehman, D. M., & Harrison, J. M. (2002). Flash visual evoked potentials in the hypomyelinated mutant mouse shiverer. *Documenta Ophthalmologica, 104*(1), 83–95.

Lickey, M. E., Pham, T. A., & Gordon, B. (2004). Swept contrast visual evoked potentials and their plasticity following monocular deprivation in mice. *Vision Research, 44*(28), 3381–3387.

Norcia, A. M., & Tyler, C. W. (1985). Infant VEP acuity measurements: Analysis of individual differences and measurement error. *Electroencephalography and Clinical Neurophysiology, 61*(5), 359–369.

Nusinowitz, S., Ridder, W. H., III, & Heckenlively, J. (2002). Electrophysiological testing of the mouse visual system. In R. S. Smith (Ed.), *Systematic evaluation of the mouse eye: Anatomy, pathology, and biomethods* (pp. 320–344). Boca Raton: CRC.

Ordy, J. M., & Samorajski, T. (1968). Visual acuity and ERG-CFF in relation to the morphologic organization of the retina among diurnal and nocturnal primates. *Vision Research, 8*(9), 1205–1225.

Peachey, N. S., & Ball, S. L. (2003). Electrophysiological analysis of visual function in mutant mice. *Documenta Ophthalmologica, 107*(1), 13–36.

Peachey, N. S., Roveri, L., Messing, A., & McCall, M. A. (1997). Functional consequences of oncogene-induced horizontal cell degeneration in the retinas of transgenic mice. *Visual Neuroscience, 14*(4), 627–632.

Peichl, L., Ott, H., & Boycott, B. B. (1987). Alpha ganglion cells in mammalian retinae. *Proceedings of the Royal Society of London Series B. Biological Sciences, 231*(1263), 169–197.

Penn, R. D., & Hagins, W. A. (1972). Kinetics of the photocurrent of retinal rods. *Biophysical Journal, 12*, 1073.

Porciatti, V., Pizzorusso, T., Cenni, M. C., & Maffei, L. (1996). The visual response of retinal ganglion cells is not altered by optic nerve transection in transgenic mice overexpressing Bcl-2. *Proceedings of the National Academy of Sciences of the United States of America, 93*(25), 14955–14959.

Porciatti, V., Pizzorusso, T., & Maffei, L. (1999a). Vision in mice with neuronal redundancy due to inhibition of developmental cell death. *Visual Neuroscience, 16*(4), 721–726.

Porciatti, V., Pizzorusso, T., & Maffei, L. (1999b). The visual physiology of the wild type mouse determined with pattern VEPs. *Vision Research, 39*(18), 3071–3081.

Prusky, G. T., Alam, N. M., Beekman, S., & Douglas, R. M. (2004). Rapid quantification of adult and developing mouse spatial vision using a virtual optomotor system. *Investigative Ophthalmology & Visual Science, 45*(12), 4611–4616.

Prusky, G. T., West, P. W., & Douglas, R. M. (2000). Behavioral assessment of visual acuity in mice and rats. *Vision Research, 40*(16), 2201–2209.

Remtulla, S., & Hallett, P. E. (1985). A schematic eye for the mouse, and comparisons with the rat. *Vision Research, 25*(1), 21–31.

Ren, J. C., LaVail, M. M., & Peachey, N. S. (2000). Retinal degeneration in the nervous mutant mouse. III. Electrophysiological studies of the visual pathway. *Experimental Eye Research, 70*(4), 467–473.

Ridder, W., 3rd., Nusinowitz, S., & Heckenlively, J. R. (2002). Causes of cataract development in anesthetized mice. *Experimental Eye Research, 75*(3), 365–370.

Ridder, W. H. 3rd., (2004). Methods of visual acuity determination with the spatial frequency sweep visual evoked potential. *Documenta Ophthalmologica, 109*(3), 239–247.

Ridder, W. H., 3rd., McCulloch, D., & Herbert, A. M. (1998). Stimulus duration, neural adaptation, and sweep visual evoked potential acuity estimates. *Investigative Ophthalmology & Visual Science, 39*(13), 2759–2768.

Ridder, W. H., 3rd, & Nusinowitz, S. (2002). Sweep VEP (sVEP) acuity in mice [abstract]. *2002 Annual Meeting Abstract and Program Planner [on CD-ROM]. Association for Research in Vision and Ophthalmology. Abstract 1802*.

Rossi, F. M., Pizzorusso, T., Porciatti, V., Marubio, L. M., Maffei, L., & Changeux, J. P. (2001). Requirement of the nicotinic acetylcholine receptor beta 2 subunit for the anatomical and functional development of the visual system. *Proceedings of the National Academy of Sciences of the United States of America, 98*(11), 6453–6458.

Schmucker, C., Seeliger, M., Humphries, P., Biel, M., & Schaeffel, F. (2005). Grating acuity at different luminances in wild-type mice and in mice lacking rod or cone function. *Investigative Ophthalmology & Visual Science, 46*(1), 398–407.

Schroeder, C. E., Tenke, C. E., & Givre, S. J. (1992). Subcortical contributions to the surface-recorded flash-VEP in the awake macaque. *Electroencephalography and Clinical Neurophysiology, 84*(3), 219–231.

Schroeder, C. E., Tenke, C. E., Givre, S. J., Arezzo, J. C., & Vaughan, H. G. Jr., (1991). Striate cortical contribution to the surface-recorded pattern-reversal VEP in the alert monkey. *Vision Research, 31*(7–8), 1143–1157.

Stone, C., & Pinto, L. H. (1993). Response properties of ganglion cells in the isolated mouse retina. *Visual Neuroscience, 10*(1), 31–39.

Strain, G. M., & Tedford, B. L. (1993). Flash and pattern reversal visual evoked potentials in C57BL/6J and B6CBAF1/J mice. *Brain Research Bulletin, 32*(1), 57–63.

Strasburger, H., Scheidler, W., & Rentschler, I. (1988). Amplitude and phase characteristics of the steady-state visual evoked potential. *Applied Optics, 27*, 1069–1088.

Sun, W., Li, N., & He, S. (2002). Large-scale morphological survey of mouse retinal ganglion cells. *Journal of Comparative Neurology, 451*(2), 115–126.

Szel, A., Lukats, A., Fekete, T., Szepessy, Z., & Rohlich, P. (2000). Photoreceptor distribution in the retinas of subprimate mammals. *Journal of Optical Society of America A, Optics, Image Science, and Vision, 17*(3), 568–579.

Tebano, M. T., Luzi, M., Palazzesi, S., Pomponi, M., & Loizzo, A. (1999). Effects of cholinergic drugs on neocortical EEG and flash-visual evoked potentials in the mouse. *Neuropsychobiology, 40*(1), 47–56.

Van der Marel, E. H., Dagnelie, G., & Spekreijse, H. (1984). Subdurally recorded pattern and luminance EPs in the alert rhesus monkey. *Electroencephalography and Clinical Neurophysiology, 57*(4), 354–368.